Solar Energy Materials & Solar Cells 161 (2017) 407–415

Contents lists available at ScienceDirect

Solar Energy Materials & Solar Cells

journal homepage: www.elsevier.com/locate/solmat

Stability and reliability of P3HT:PC61BM inverted organic solar cells

Nikhil Chander[a,1], Sujata Singh[b,2], S. Sundar Kumar Iyer[a,c,*]

[a] National Centre for Flexible Electronics, Indian Institute of Technology, Kanpur, Kanpur 208016, Uttar Pradesh, India
[b] Dynotech Instruments Pvt. Ltd., New Delhi 110058, India
[c] Department of Electrical Engineering, Indian Institute of Technology, Kanpur, Kanpur 208016, Uttar Pradesh, India

ARTICLE INFO

Keywords:
Organic photovoltaics
Inverted organic solar cells
Stability and reliability
Shelf lifetime
Outdoor testing
Thermal stability

ABSTRACT

Improving the stability and reliability of organic photovoltaic (OPV) devices is an area of intense research as it is the major barrier in the commercialization of these devices. We study the stability of inverted structured OPV devices in the present work. A large number of these were fabricated and their shelf life times were recorded. P3HT devices show an average T80 (time in which cell efficiency falls to 80% of its initial value) of 34 days. Some of the devices were tested in actual working conditions outdoors in sunlight. A very low T80 value of 12 h was observed during the outdoor testing. Thermal degradation study was performed on the devices at 65 °C in dark and an average T80 of 200 h was obtained. Signatures of trap formation were observed by analysing and comparing the dark current-voltage characteristics of the pristine and degraded devices. The solar cells degrade due to trap formation in the active layer and formation of charge extraction barriers at the contacts.

1. Introduction

Organic solar cells (OSCs) are promising candidates for light-weight and low-cost sources of renewable energy. OSCs also have the potential for rapid roll-to-roll processing and can be fabricated on flexible substrates. A popular form of OSC consists of an active layer blend made up of a conjugated polymer and a fullerene derivative sandwiched between two electrodes. A schematic of the popular OSC architecture is shown in Fig. 1a. Many standard structures of OSCs utilize poly(3,4- ethylenedioxylenethiophene):poly(styrenesulphonic acid) (PEDOT:PSS) as a hole transporting layer (HTL) or the electron blocking layer (EBL). The acidic nature of can lead to etching of the indium tin oxide (ITO) electrode and thus reduce the device lifetime [1]. It was found that the inverted structure is better suited for improving the stability of OSCs [1]. In this architecture, n-type metal oxides such as TiO_2 or ZnO are deposited on ITO and used as electron transport layer (ETL), while other metal oxides such as NiO, MoO_3 and WO_3 can be used as HTL [1–4]. Schematics of the inverted OSC architecture and the flat band energy levels are shown in Fig. 1b and c respectively. blend forms the active layer, and ZnO and MoO_3 are used as ETL and HTL, respectively.

The major reasons and mechanisms for degradation of OSC device performance and parameters are documented widely in literature. Humidity, oxygen, ultraviolet (UV) light and thermal stresses are known to degrade the OSC performance significantly [5–9]. The effects of these physical agents can be minimized by proper encapsulation of the device. However, since a solar cell is exposed to light and thermal stresses during its use, the degradation brought about by these stresses cannot be eliminated. Light and heat induce morphological changes in the active layer, which lead to interlayer and electrode diffusion [10,11]. In order to obtain a good insight of device stability, it is essential to study the complete working device under various stresses and observe how the different photovoltaic (PV) parameters evolve with time.

Almost all previous works on stability focussed on standard architecture OPV devices [5–14]. In the present work, we studied the stability of inverted structured OSCs based on P3HT: PC61BM active layer. To obtain statistically significant data sets, more than 90 encapsulated substrates with four devices each were fabricated and their shelf life times were recorded. Some of the devices were stressed in actual outdoor conditions in sunlight to find out the photo-stability and lifetime under light exposure. In addition, some devices were thermally stressed in dark ambient conditions to study the effect of temperature on the device performance. The performances of inverted OSCs were analysed using current density-voltage (*J-V*, measured under solar simulator) and external quantum efficiency (EQE) measurements. Dark current-voltage (*I-V*) analysis has also been performed to observe charge carrier trap signatures in the OSCs.

* Corresponding author at: Department of Electrical Engineering, Indian Institute of Technology, Kanpur, Kanpur 208016, Uttar Pradesh, India.
E-mail addresses: nikhilphysics@gmail.com (N. Chander), sskiyer@iitk.ac.in (S.S.K. Iyer).
[1] Author's present affiliation: CSIR-National Physical Laboratory, Dr. K.S. Krishnan Road, New Delhi-110012, India.
[2] Second Author (Ms. Sujata Singh) contributed to the work reported here when she was working for MNRE supported project 31/18/2009-10/PVSE at IIT Kanpur.

http://dx.doi.org/10.1016/j.solmat.2016.12.020
Received 21 August 2016; Received in revised form 24 October 2016; Accepted 10 December 2016

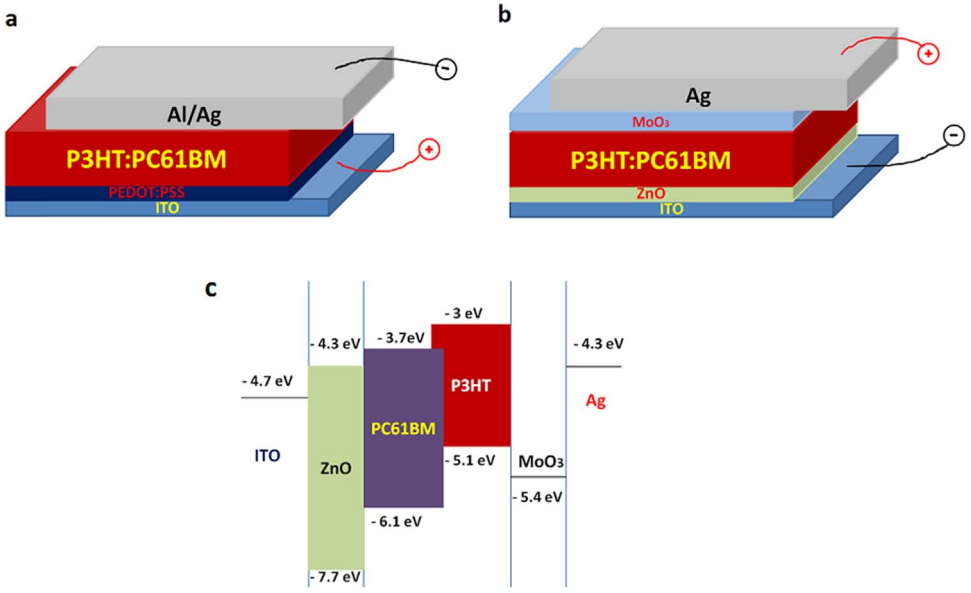

Fig. 1. (a) Standard OPV structure for P3HT:PC61BM as the active layer. (b) A schematic of the inverted organic solar cell architecture fabricated in the present work. (c) Schematic energy levels of the inverted device under open-circuit (flat-band) conditions.

2. Experimental

2.1. Device fabrication

Electron donor polymer P3HT and fullerene electron acceptor PC61BM were purchased from Sigma Aldrich and used as received without any purification. The inverted OSC structure was a stack of ITO/ZnO/P3HT:PC61BM/MoO_3/Ag layers. The ITO substrates of size 5 cm were patterned using photolithography technique to obtain four different sizes of ITO strips. Patterned ITO substrates were cleaned sequentially in soap water, de-ionized water and propanol. The cleaned ITO substrates were subjected to oxygen plasma treatment prior to device fabrication. A thin layer (~30 nm) of ZnO was formed by spin coating at 3000 rpm a solution of zinc acetate and 2-methoxyethanol on top of ITO. The ZnO coated substrates were annealed in air at 250 °C for 15 min and transferred to a N_2 filled glove-box for further processing. The active layer materials P3HT/PC61BM were dissolved in dichlorobenzene in 1:1 wt ratio and a concentration of 20 mg/ml. This solution was dropped on ZnO coated ITO substrates using a glass syringe attached with a 0.45 µm Polyvinylidene Difluoride (PVDF) filter. The active layer was then spin coated at 500 rpm for 1 min for obtaining a targeted final thickness of ~120 nm. The active layer coated substrates were annealed inside the glove box at 110 °C for 30 min and subsequently transferred to a glove box integrated thermal evaporator for MoO_3 and Ag deposition. A thin (~ 3 nm) layer of MoO_3 was deposited using shadow masks. The thickness of deposited Ag electrode was ~100 nm. This completed the device fabrication and cell pixels of four different areas were obtained: C1 (0.7 cm), C2 (1 cm), C3 (1.2 cm) and C4 (1.3 cm). These pixels were characterised by covering with square metallic masks to define four different active areas: A1 (0.5 cm), A2 (0.7 cm), A3 (0.9 cm) and A4 (1 cm). In the subsequent sections of this paper, the devices C1, C2, C3 and C4 refer to cells with active areas 0.25 cm^2, 0.49 cm^2, 0.81 cm^2 and 1 cm^2, respectively (see supplementary **Fig. S1**).

2.2. Encapsulation of organic solar cells

Encapsulation is a critical step in device processing and determines, to a great extent, its stability and reliability in actual working conditions. The devices were encapsulated using a grooved glass and UV-curable epoxy glue (Epoxy Technology, USA). The encapsulation process was performed inside the glove box using a semi-automated system. Initially, grooved glasses were cleaned by sonicating them in DI water, isoprapanol and acetone for 10 min each. Afterwards, the grooved glasses were dried using a nitrogen gun and transferred to a nitrogen filled glove box housing the semi-automatic encapsulation system. Epoxy glue was applied on the grooved glass using a robotic dispenser. The grooved glass with epoxy and the solar cell substrate were aligned manually with the help of custom made holders. The aligned glass and device were pressed together using a mechanical press and kept under a UV lamp for 2 min. The epoxy was cured by UV rays to which it was exposed, solidifying the initially liquid epoxy. The cured epoxy held together the grooved glass and the solar cell substrate. The epoxy layer was expected to be a barrier against oxygen and moisture ingress into the device.

2.3. Device characterization

The PCEs of the fabricated PTB7 and P3HT devices were determined from current density-voltage (*J-V*) curves measured using Keithley 2400 source-meter under 1 sun AM1.5 G illumination from a solar simulator (Class AAA, Newport-Oriel, USA). The illumination intensity was adjusted using a calibrated reference silicon solar cell. To ensure well defined active areas, the *J-V* measurements were performed using laser-cut stainless steel square masks. Incident photon to current conversion efficiency (IPCE) of inverted OSCs was measured using a custom-built apparatus consisting of a tungsten lamp, monochromator, chopping wheel, lock-in amplifier and current pre-amplifier. The incident monochromatic light was chopped at 11 Hz and the measurements were taken in the range 330–850 nm with an interval of 5 nm. All the measurements were performed at room temperature in ambient conditions.

2.4. Stability testing of organic solar cells

Stress testing of OSCs to study their aging process was carried out according to the consensus stability testing protocols defined by Reese et al. [15]. Three sets of experiments were performed. In the first case, the shelf lifetime of inverted OSCs based on PTB7 and P3HT were compared. In the second case, the OSCs were placed outdoors and their photovoltaic (PV) parameters were studied periodically. In the third set of experiment, the OSCs were stored at 65 °C in the dark. The PV

Table 1
Overview of the three types of test protocols adopted in the present work.

Test type	Dark	Outdoor	Dark
Test ID	ISOS-D–1 Shelf	ISOS-O–1 Outdoor	ISOS-D–2 High temperature storage
Light source	None	Sunlight	None
Temperature	Ambient	Ambient	65/85 °C (65 °C in present case)
Relative Humidity (RH)	Ambient	Ambient	Ambient
Environment/Setup	Ambient	Outdoor	Hot plate/oven (Hot plate in present case)
Characterization light source	Solar simulator	Solar simulator	Solar simulator
Load	Open-circuit	Open-circuit	Open-circuit

parameters: short-circuit current density (J_{SC}), open-circuit voltage (V_{OC}), fill factor (FF) and power conversion efficiency (PCE), were recorded before and after the experiments to evaluate the performance of OSCs under varying stress conditions. Table 1 summarizes the type of experiment and the related ISOS consensus stability protocol [15].

3. Results and discussion

3.1. Shelf life-time of inverted organic solar cells

The study of performance degradation of inverted OSCs was carried out according to the ISOS-D-1 Shelf protocol [15]. The PV parameters of the inverted devices were measured immediately after their fabrication and the subsequently measured parameters were normalized with respect to the initial values. The cells were stored in dark under ambient conditions between the measurements. In the present work, the solar cell life time is defined as the time in which the cell efficiency falls to 80% (T80) of the initial efficiency (measured immediately after the device fabrication). T90 values, time in which efficiency falls to 90% of the initial value, are also reported.

In order to accurately predict the lifetime of OSCs, it is imperative to have a large number of devices so that a statistically significant dataset can be obtained [16,17]. The devices used in the present study were fabricated over several weeks. Typically each week three substrates were fabricated. Each substrate had four devices C1, C2, C3 and C4 of area 0.25 cm^2, 0.49 cm^2, 0.81 cm^2 and 1 cm^2, making a total of twelve individual devices fabricated per week (see also supporting information **Fig. S2**). Data for 26 weeks were obtained from 78 different P3HT substrates with a total 312 devices (see Table 2). Some devices suffered physical damage while handling during fabrication or characterization and the final numbers of pixels of each type available for analysis are mentioned in the table footnotes.

The lifetimes (T90 and T80) of inverted P3HT solar cells for devices with different areas are shown in Fig. 2. The overall average T90 of

Table 2
Initial photovoltaic parameters of inverted organic solar cell devices used for shelf-life test. Average values along with standard deviations are reported for four different area cells.

Cell/Area	J_{SC} (mA·cm^{-2})	V_{OC} (V)	Fill Factor (%)	Efficiency (%)
C1/0.25 cm^2[a]	8.55 ± 1.10	0.60 ± 0.11	53.7 ± 10. 6	2.89 ± 0.98
C2/0.49 cm^2[b]	8.44 ± 1.25	0.61 ± 0.08	49.8 ± 11.4	2.63 ± 0.90
C3/0.81 cm^2[c]	7.46 ± 1.64	0.57 ± 0.16	48.0 ± 11.5	2.26 ± 1.01
C4/1 cm^2[d]	7.69 ± 1.50	0.59 ± 0.13	48.3 ± 10.5	2.37 ± 0.86

[a] One device was shorted and six suffered physical damage; this data is for 71 devices.
[b] Four devices were shorted and six suffered physical damage; this data is for 68 devices.
[c] Three devices were shorted and six suffered physical damage; this data is for 69 devices.
[d] Six devices were shorted and six suffered physical damage; this data is for 66 devices.

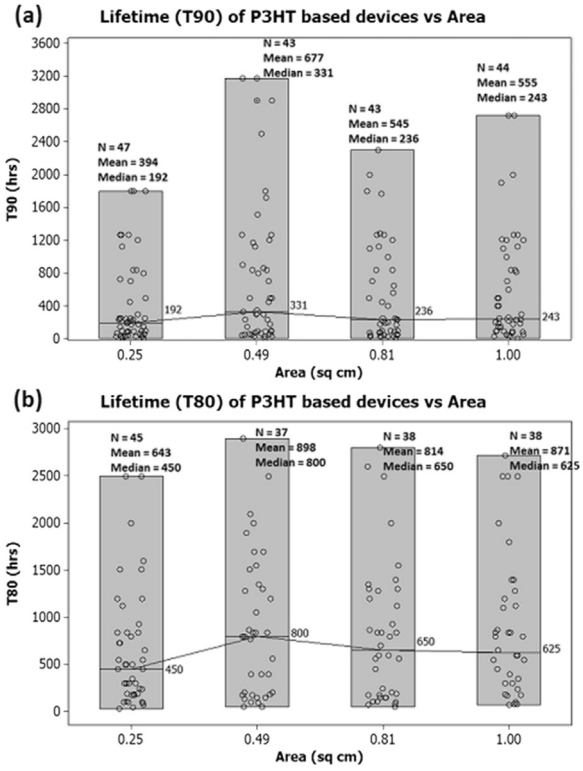

Fig. 2. (a) T90 and (b) T80 lifetimes of P3HT devices for four different areas.

P3HT devices (including all four device areas) is 543 h, which is approximately 23 days. It implies that the initial efficiency is reduced to 90% in less than a month, when the devices are stored in the dark. The median T90 values are much less than the mean values as seen in Fig. 2a. It shows that majority of the devices have a T90 value lower than the mean value of 23 days.

Similarly, the overall average T80 of the P3HT devices (including all four device areas) is 807 h or approximately 34 days. This data may be pessimistic as it does not reflect the devices as some of the 'good' cells did not reach T80 even at the time of compiling the results.

The histogram in Fig. 3a shows the distribution of data points in the efficiency bins and the histogram in Fig. 3b shows distribution of data points in lifetime (T80) bins. The total frequency counts in Figs. 3a and 3b are 274 and 158 respectively. There were 58 devices (about 21% of the total 274 devices) which had not reached T80 at the time of compilation of results. Also, 36 devices (about 13% of the total) fabricated during the last 3 weeks of the study did not reach T90. Five substrates (20 devices, about 7% of the total) were physically damaged during repeated characterizations. Physical damage included catastrophic failures like detachment of encapsulation glass and breakage of the solar cell substrate itself. The data shown in Fig. 3b correspond to 158 devices that reached T80.

It is clear from the graphs that majority of the devices degrade in the first month itself, although some devices last more than 3 months in dark storage. Such a large difference in T80 of similarly processed devices can be because of several factors. However, the primary reason is the variation in the manual fabrication process itself. Since all the steps require partial or complete human involvement, the thicknesses and uniformities of active layer have variations for devices fabricated in different batches. The encapsulation process, though automated in some aspects, requires manual placing of encapsulation glass over the solar cell substrate. It has been noticed by visual inspection that the good devices, with a T80 of more than 45 days, have very good encapsulation. On the other hand, devices with low T80 values had air pockets and holes in the epoxy layer used for encapsulation. This emphasises the need to have a good and stable encapsulation process to

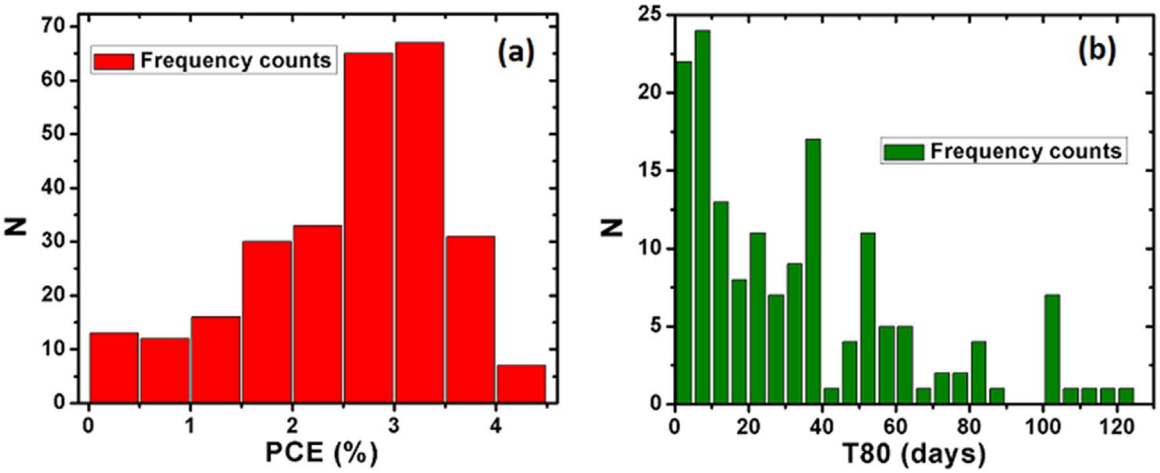

Fig. 3. Histogram of data points of P3HT:PC61BM cells in (a) efficiency bins and (b) lifetime (T80) bins.

achieve best possible lifetime.

As a representative example, the data of a P3HT cell which has a T80 of 37 days that is close to the average T80 value of inverted P3HT devices is reported in the present work. Fig. 4a shows the time evolution of PV parameters of a 0.25 cm^2 inverted P3HT: PC61BM solar cell. Fig. 4b shows the time variation of semi-log dark *I-V* curve of the cell, while the light *J-V* curves are plotted in Fig. 4c. EQE variation of the cell is shown in Fig. 4d.

It can be observed from Fig. 4a that the J_{SC} and FF values are affected more than the V_{OC} values. The device has an increasingly leaky behaviour as seen from the dark *I-V* curves recorded at t=60 and 75 days. The decrease in generated photocurrent (light *I-V* curve) correlates strongly with the decrease in spectral response. Although, the device is somewhat stabilized after 75 days, it has already reached its T50 lifetime. The device efficiency degrades steadily with time, indicating that the encapsulation is playing a major role in preventing rapid decay in the first few days [17,18].

For P3HT devices, it has been reported earlier that reduced charge collection efficiency due to light induced trap formation in P3HT disorder domains leads to a decrease in photocurrent and fill factor [19]. The dark *I-V* characteristics are analysed and the *G* versus *V* graph using an earlier reported method [20] is re-plotted.

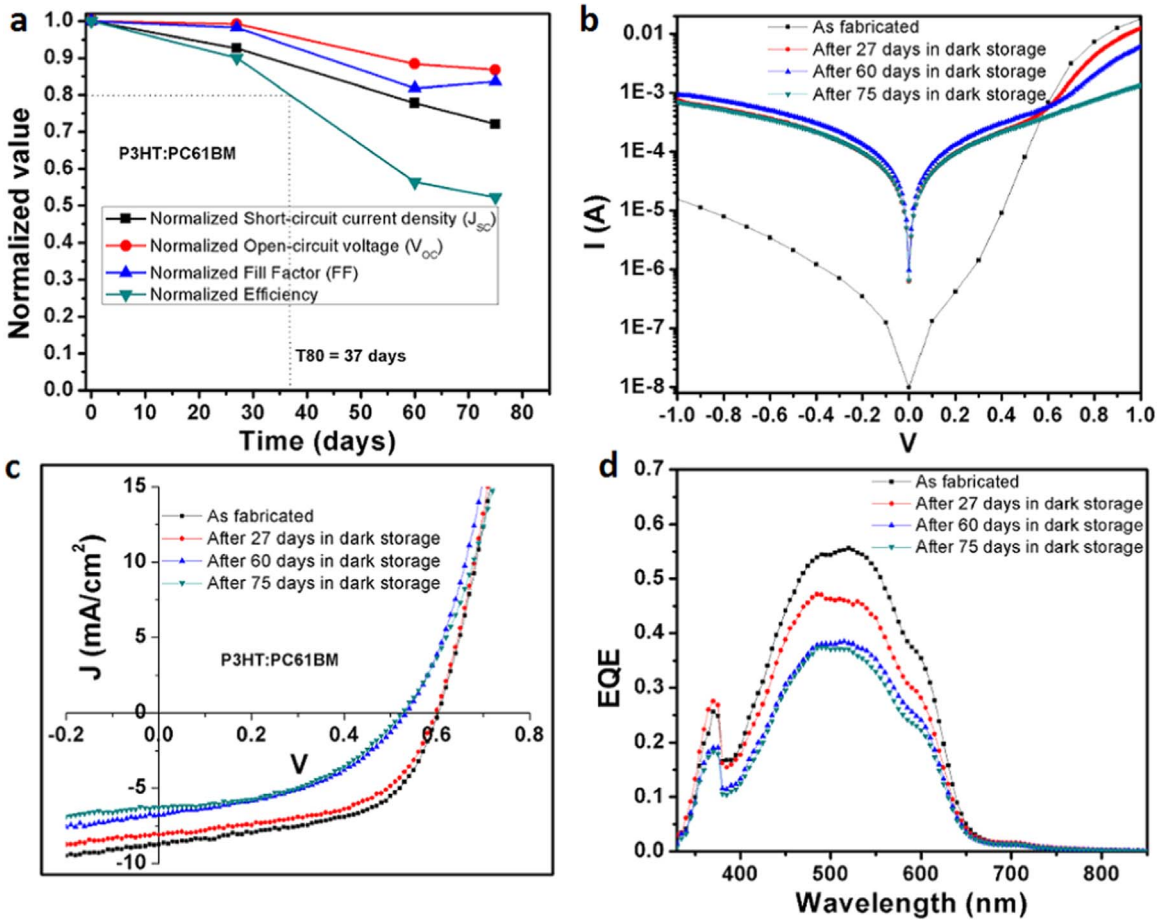

Fig. 4. Time variation of (a) normalized values of photovoltaic parameters, (b) semi-log dark *I-V* curve, (c) light *J-V* curve and (d) EQE curve of a 0.25 cm^2 P3HT:PC61BM device.

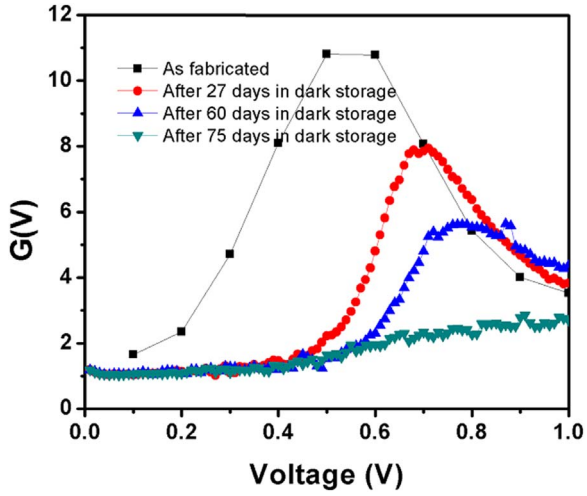

Fig. 5. *G-V* plot of dark *I-V* characteristics of P3HT:PC61BM device stored in dark.

The distortions in *I-V* characteristics arising due to presence of traps is further analysed with the help of the *G-V* plots. The function *G*(*V*) is defined as G(V)=*d* log (*I*)/*d* log (*V*), where *d* is the differential operator. This differentiation is performed using numerical values and a graph of *G* values as a function of voltage *V* is plotted. The peak observed in the graph occurs at a voltage proportional to the built-in voltage in the device. This method is based on *I-V* characteristics being power-law dependent above built-in voltage and exponentially dependent below it in a two-terminal organic diode. Traps lead to deviations in *I-V* curves of organic diodes due to their voltage dependent occupancy behaviour. The presence of traps would change the *G-V* plot in a prominent way so that it would be easily identifiable. A detailed account of *G-V* analysis is beyond the scope of this work but qualitative comments based on an earlier work by Rizvi et al. have been given at appropriate places [20]. Increase in trap signatures for our device stored in dark are observed (see Fig. 5). As the device degrades, the peak in the *G-V* curve drops and becomes less prominent. Also, the *G-V* graph loses its shape and appears stretched out. This is an indication of increasing trap concentration which correlates with the reduction in photocurrent and fill factor. This behaviour is typical of Gaussian distributed traps in the energy gap with concentration *N* and variance σ with the following distribution [20]: $g(E)=\frac{N}{\sigma\sqrt{2\pi}}\exp\left(-\frac{1}{2}\frac{(E-E_t)^2}{\sigma_t^2}\right)$

Here, E_t is the energy within the bandgap at which the Gaussian trap distribution peaks. These trap formations with time in the device active layers is a major reason for device degradation.

For comparison, a device with relatively bad encapsulation is shown in Fig. S3. In the first two days following the device fabrication, the efficiency drops to 80% of the initial value. All the photovoltaic parameters register a decline during this period. On the other hand, the good encapsulation device shown in Fig. 4 reaches T80 after 37 days in dark storage. The quality of encapsulation is the major difference between the two devices. A device with poor encapsulation degrades very fast initially while the device with good encapsulation doesn't show such behaviour. The device with poor encapsulation reaches T50 in 40 days compared to 75 days for the good encapsulation device (see Fig. S3 and Fig. 4a). Proper encapsulation is of prime importance to attain stable and reliable OPV devices.

3.2. Outdoor testing of inverted organic solar cells

Outdoor field testing is the most important type of stress testing for OSCs as it can give a realistic value of device lifetime [15,17]. The outdoor light experiments were performed in early-April 2016. The Indo-Gangetic plain in North India (where Kanpur is located) receives a lot of sunshine in April and the sky is relatively clear during this month [21]. The maximum day temperature during this month generally stays below 40 °C. These conditions are very suitable for outdoor testing of solar cells to study the effect of photo-degradation [22].

The OSCs were placed outdoors in IIT-Kanpur campus (coordinates - 26.51°N, 80.23°E) on an inclined surface facing the sun. The samples were manually adjusted periodically to ensure that the sun rays were incident almost perpendicular to the solar cells. The PV parameters were recorded periodically with a solar simulator by bringing devices inside the lab for the measurement. The samples were placed outside at 10:30 AM and brought indoors at 4 PM on test days. A total of 20 devices (five substrates with four devices each) were tested in this fashion. Fig. 6 shows the data points for the 20 devices in efficiency and lifetime (T80) bins.

The T80 lifetime values range from 9 to 19 h as seen in Fig. 6b. A majority of the devices have a T80 of 11 h. The degradation in the first 10–15 h was more severe as seen from Fig. 7a. But even after this drastic initial degradation, the efficiency continued to drop, almost linearly and did not stabilize. In fact, all the 20 devices had degraded to less than 60% of their initial efficiencies after 45 h of outdoor testing. All the PV parameters, except V_{OC}, decreased steadily resulting in efficiency degradation.

The dark *I-V* plot is shown in semi-log scale in Fig. 7b. In the degraded device, the reverse current is higher and forward current at +1 V is marginally lower than the pristine device. These observations, along with the *G-V* plot shown in Fig. 8, are indicative of light-induced

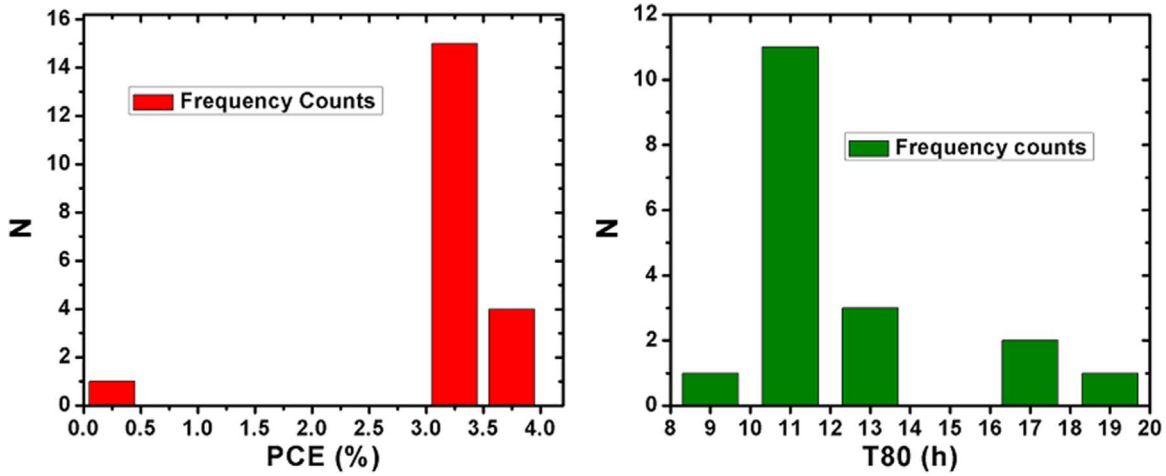

Fig. 6. Histogram of data points of P3HT:PC61BM cells tested outdoors in (a) efficiency bins and (b) lifetime (T80) bins.

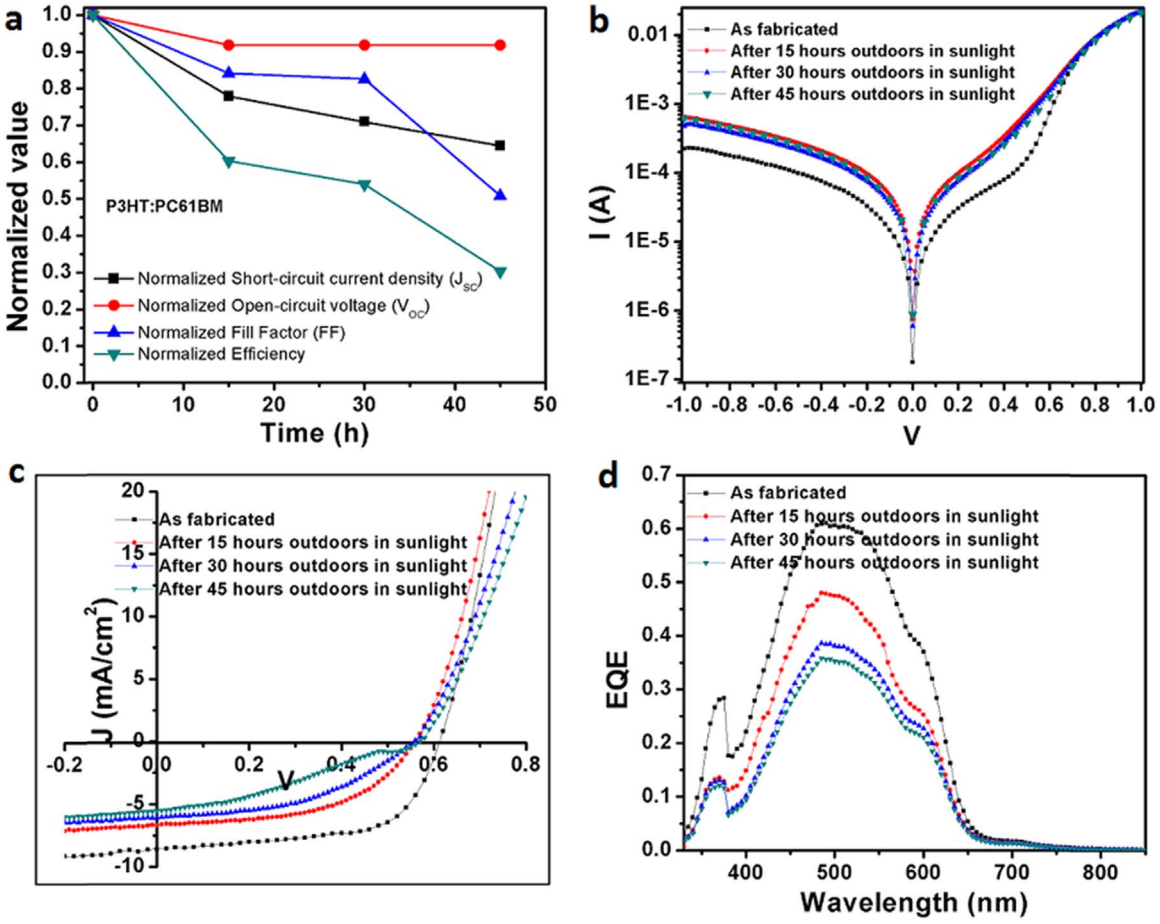

Fig. 7. Time variation of (a) normalized values of photovoltaic parameters, (b) semi-log dark *I-V* curve, (c) light *J-V* curve and (d) EQE curve of a 0.25 cm^2 P3HT:PC61BM device kept outdoors in sunlight for 45 h.

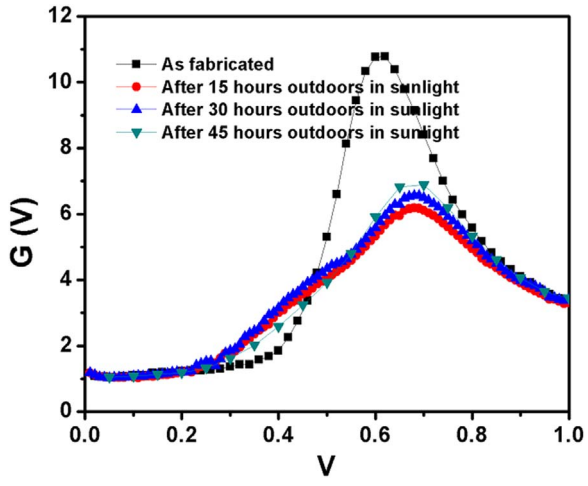

Fig. 8. *G-V* plot of dark *I-V* characteristics of P3HT:PC61BM device kept outdoors in sunlight.

trap formation in the active layer. After 45 h of outdoor light stress, an S-shape was observed in the *J-V* characteristics curve determined under a solar simulator in the laboratory conditions (light *J-V* characterises). On the other hand, for the samples studied for shelf life, the S-shape was not observed in the light *J-V* characteristics – including for those tested after 75 days in the dark. On the other hand, for devices kept outdoors in sunlight, the S-shape in the light *J-V* characteristics appeared after only 45 h. So, it is inferred that the light induced stress is responsible for the observed S-shape in the light *J-V* characteristics.

The S-shape in the light *J-V* characteristics of a solar cell could happen due to the formation of charge extraction barriers at the contacts which lower the charge extraction efficiency in the device [23,24]. It has been demonstrated using electrical impedance spectroscopy that a corroded metal contact could lead to a decrease in hole extraction capability of the solar cell, which lowers the FF and PCE of the device [23,24]. Thus, it is likely that outdoor exposure of the devices is leading to the degradation of the metal semiconductor interface.

The EQE values following the outdoor field testing for 45 h, also show drastic reduction, as observed in Fig. 7(d). The *G-V* plot shown in Fig. 8 also shows signatures of trap formation with Gaussian distribution as the peak position is shifted to higher voltages and the graph is depressed and stretched [20]. Due to light stress, the changes in *G-V* plot manifest themselves very early. In the case of dark storage, the trap signatures become evident after several days, while significant degradation can be seen for the samples kept outside for only 15–45 h (Fig. 8). These results seem to be indicative of damage to the active layer. In a recent study, the reduced performance of P3HT based OSCs was attributed to deterioration in charge collection due to light induced trap formation in the active layer. The loss in V_{OC} can also be explained by the formation of deep trap sites which result in charge recombination [19].

3.3. High temperature storage in dark

Stability of OSCs under temperature stress is an important requirement of practical deployment of these devices. Here, the thermal

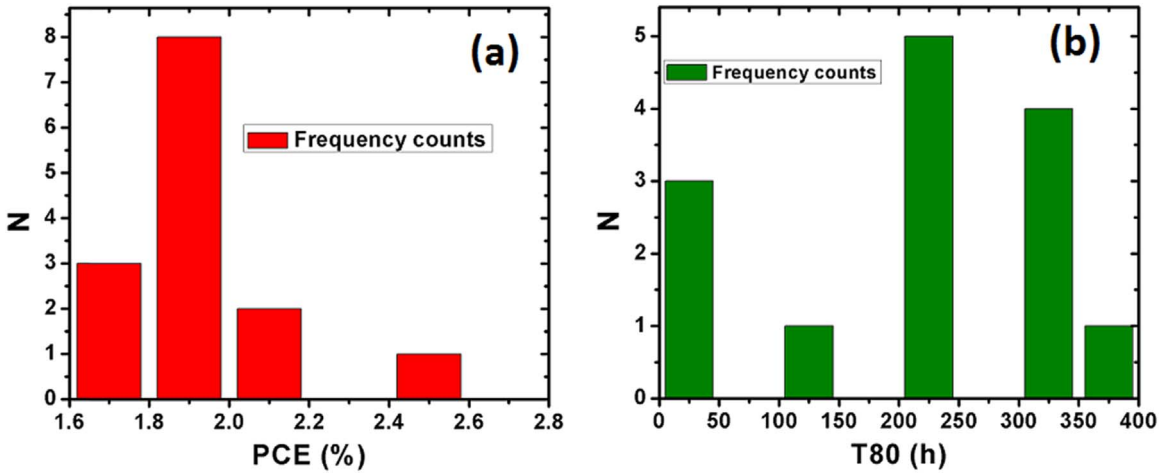

Fig. 9. Histogram of data points of P3HT:PC61BM cells stored in dark at 65 °C in (a) efficiency bins and (b) time bins.

stability of OSCs is studied by storing them in dark at 65 °C - which is the standard temperature for studying thermal degradation [15,25]. It has been previously observed that thermal degradation begins at the glass transition temperature (T_g) of the active layer blend [25]. For P3HT: PC61BM blend, the T_g value is about 56 °C for the polymer [25,26] and so the 65 °C temperature chosen for the thermal stress is above T_g.

The samples being tested were kept on a hotplate at 65 °C and in the dark. The light *J-V* characteristics of the devices were determined periodically. A total 14 devices (four substrates with four devices each with two damaged devices) were tested in this fashion. Fig. 9 shows the data points of 14 devices in efficiency and lifetime (T80) bins. Most of the devices have a T80 of more than 200 h, with one device reaching a T80 of 364 h. There were three devices which degraded very fast and reached T80 in 34 h.

In standard device architecture, the thermal degradation occurs due to the formation of a thin polymer layer at the back contact which creates a barrier for electron extraction at the organic-metal back contact interface [25]. Formation of hole-transporting polymer layer at the back metal contact is not harmful for inverted architecture devices because the back electrode acts as a hole collector.

In fact, for the first 6–8 h of heating in the dark at 65 °C, the inverted devices show an enhancement in PCE due to an improvement in J_{SC} and FF (see the inset of Fig. 10). The improvement may be because of morphological improvements of the thin active layer. The

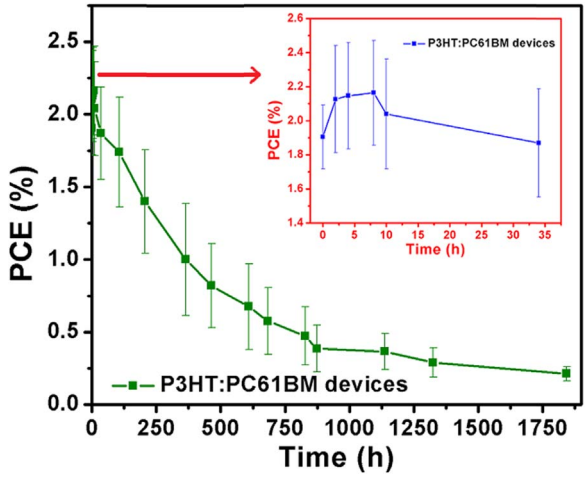

Fig. 10. Time variation of power conversion efficiencies of 14 devices that were tested for thermal degradation. Average values, along with standard deviations, are plotted from 0 to 1844 h.

average T80 value for the 14 devices was 200 h, which is very good when compared with similar works reported earlier [25,27].

The curve fitting for the thermal decay of PCE shown in Fig. 10 was performed using the equation:

$$PCE = PCE_0 + A1 * \exp(-t/t) \quad (1)$$

The obtained time constant, τ (the lifetime at which the PCE value decreases by a factor *e*), was 444.3 h (see supporting information, **Fig. S4**). It shows that the inverted devices are thermally more stable than the standard architecture devices [25,27].

Morphological characterizations were not carried out as a part of this study. Since the devices were encapsulated, morphological analysis required manual breaking of the encapsulation which, with the facilities we had access, could have completely damaged the device. Earlier studies report that the morphology changes take place in the active layer and at the electrode interfaces [25,27] for this type of thermal degradation. The stresses on the devices in this study were along similar lines to that reported in literature. Therefore, here too, we expect the degradation in device efficiency because of prolonged heating to be due to morphological changes in the active layer and due to the changes at the active layer-electrode interfaces [25,27]. The J_{SC} decreases due to morphology changes occurring in the active layer blend that can adversely affect the charge mobility and generation of charge transfer complex [10,28]. The V_{OC} reduces due to different donor/acceptor (D:A) phase segregation and increased recombination occurring as a result of increased defect states [29,30]. These factors can also decrease FF due to poor charge transport and increased series resistance and decreased shunt resistance due to recombination of carriers.

The variation of PV parameters with time, dark *I-V* and light *J-V* curves and EQE curves of a representative device are shown in Fig. 11. The initial PV parameters of the representative device are: J_{SC}=9.33 mA cm^{-2}, V_{OC}=0.62 V, FF=69% and PCE=3.98%. The initial degradation of these parameters is very rapid, but after first the 16 h of heating the degradation rate becomes slow and the device appears to stabilize. But, even then the device degrades to ~47% of its initial efficiency in 90 h. The light *J-V* and EQE curves show a decreasing trend with time, indicating that the generated photocurrent is falling because of active layer degradation and trap formation. The dark *I-V* curves, however, do not show a similar trend. Although, the *G-V* plot shown in Fig. 12 confirms that the traps are formed as the device is heated, but, surprisingly, the worst case trap generation is in the first 16 h. The initial heating for 16 h is causing a rapid burn-in of the device and later the device stabilizes. It seems that following the initial burn-in, the device recovers and some of the traps are filled after the heating is stopped. This could be a beneficial effect of initial annealing

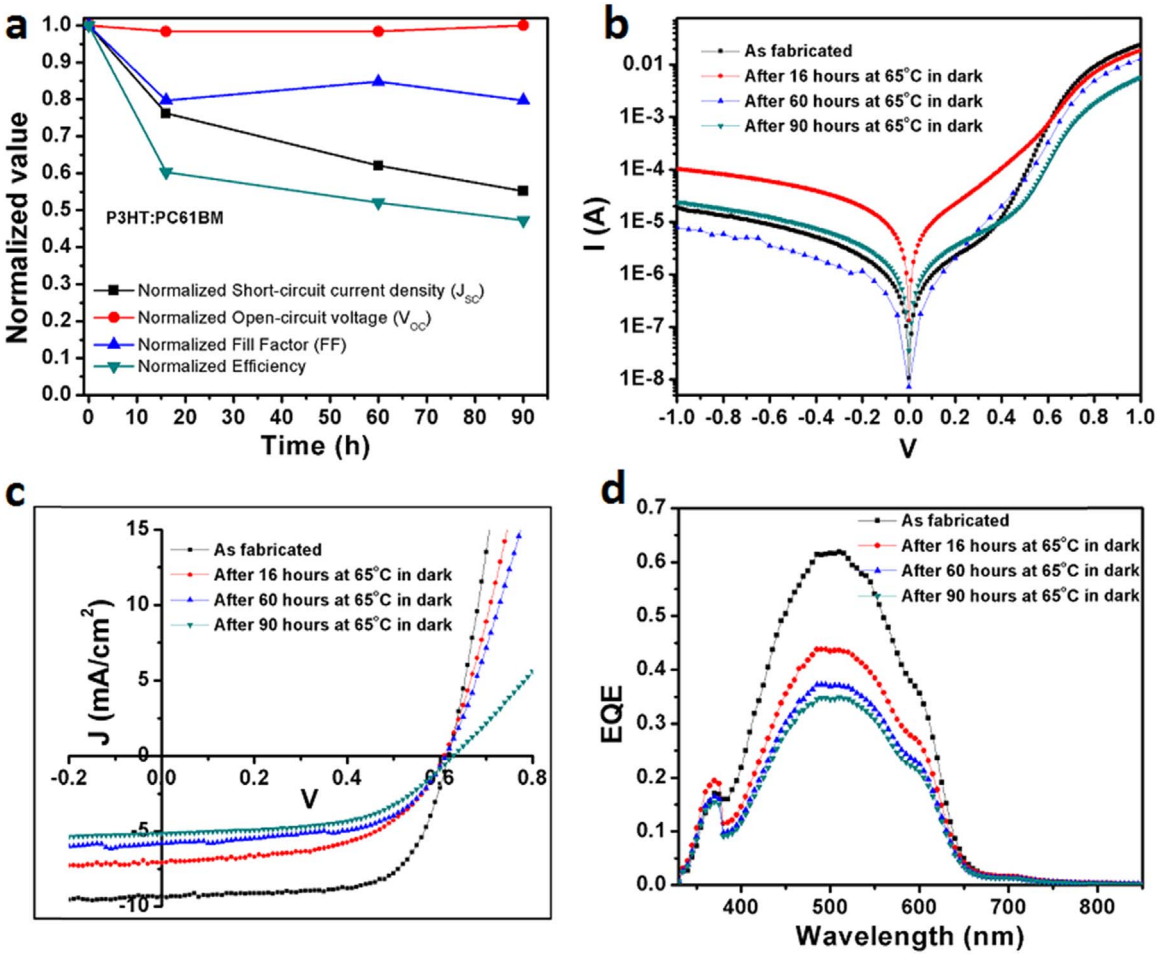

Fig. 11. Time variation of (a) normalized values of photovoltaic parameters, (b) semi-log dark *I-V* curve, (c) light *J-V* curve and (d) EQE curve of a 0.25 cm^2 P3HT:PC61BM device heated at 65 °C for 90 h in dark.

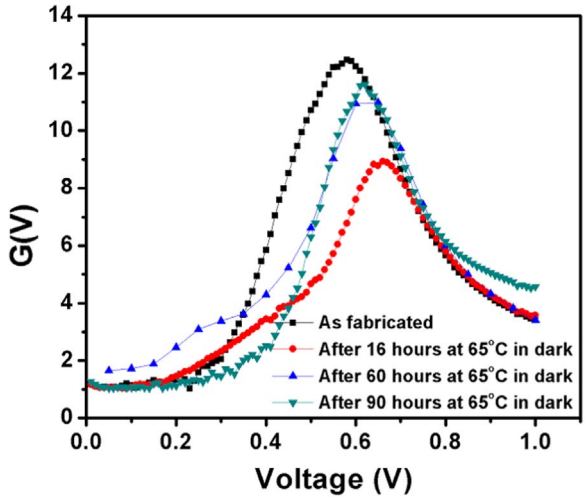

Fig. 12. *G-V* plot of dark *I-V* characteristics of P3HT:PC61BM device under thermal stress.

because subsequent annealing experiments for longer durations do not show such a drastic degradation. Further detailed studies are needed to gain more insight into this degradation behaviour.

The inverted devices employ a thin film of MoO_3 as HTL. In a recent study, the unintentional doping caused by diffusion of MoO_3 in the active layer was shown to adversely affect the device performance. It was reported that the MoO_3 doping could weaken charge transport and increase trap-assisted recombination in OSCs based on polymer-fullerene blends [31]. Further experimentation is needed to study the effects of MoO_3 and other carrier selective layers on the stability of OSCs. It can be considered an active research area in the near future.

4. Conclusion

For a first of its kind study in India, a reliable and stable process line for fabricating encapsulated inverted OSCs was set up and hundreds of devices were fabricated. Statistical evaluation of the shelf life-time data for inverted OSCs showed that a significant proportion (more than 40%) of the cells had a T80 of more than one month. There were 11 devices which lasted more than three months. Improved encapsulation strongly appears to be critical for longer life. Outdoor testing of the devices was found to be the most severe test condition and all the 20 tested devices degraded to less than 60% of their initial efficiencies after 45 h of outdoor sunlight exposure. Signatures of metal semiconductor interface degradation are strongly evident for this stress. Thermal degradation time constant at 65 °C was determined to be 444 h. During this stress, morphological changes in the active layer and changes at the active layer-electrode interfaces causes the devices to degrade. Better encapsulation, more photo-stable materials and robust active layer-electrode interfaces are required to fully exploit the advantages of the inverted device architecture.

Acknowledgments

We thank Ministry of New and Renewable Energy (MNRE), Govt. of

India for financial support through the project. The support of the whole MNRE project team at SCDT and especially the technical help provided by Mr. Eswaran Jayaraman and Ms. Madhu Rawat in the present study is also acknowledged. Some of the later results in the paper was possible due to financial support from Department of Electronics and Information Technology, Government of India through the "Centre of Excellence for Large Area Flexible Electronics", Administrative Approval No. 2(4)/2014-PEGD dated 14.11.2014. One of the authors (Dr. Nikhil Chander) would like to thank Department of Science & Technology, Government of India for financial support during the writing of this paper through INSPIRE Faculty Award number.

References

[1] Z. He, C. Zhong, S. Su, M. Xu, H. Wu, Y. Cao, Enhanced power-conversion efficiency in polymer solar cells using an inverted device structure, Nat. Photon 6 (2012) 591–595.
[2] Z. Lin, C. Jiang, C. Zhu, J. Zhang, Development of inverted organic solar cells with TiO_2, Interface Layer. Using Low-Temp. At. Layer Depos. Appl. Mater. Interfaces 5 (3) (2013) 713.
[3] Y. Sun, Ch.J. Takacs, S.R. Cowan, J. Hwa Seo, X. Gong, A. Roy, A.J. Heeger, Efficient, Air-stable bulk heterojunction polymer solar cells using MoO_x as the anode interfacial layer, Adv. Mater. 23 (19) (2011) 2226.
[4] J. You, C.C. Chen, L. Dou, S. Murase, H.S. Duan, S.A. Hawks, T. Xu, H.J. Son, L. Yu, G. Li, Y. Yang, Metal oxide nanoparticles as an electron-transport layer in high-performance and stable inverted polymer solar cells, Adv. Mater. 24 (2012) 5267–5272.
[5] K. Norrman, S.A. Gevorgyan, F.C. Krebs, Water-induced degradation of polymer solar cells studied by $H_2{}^{18}O$ labeling, ACS Appl. Mater. Interfaces 1 (2009) 102–112.
[6] A. Guerrero, P.P. Boix, L.F. Marchesi, T. Ripolles-Sanchis, E.C. Pereira, G. Garcia-Belmonte, Oxygen doping-induced photogeneration loss in P3HT: pcbm solar cells, Sol. Energy Mater. Sol. Cells 100 (2012) 185–191.
[7] F.C. Krebs, S.A. Gevorgyan, J. Alstrup, A roll-to-roll process to flexible polymer solar cells: model studies, manufacture and operational stability studies, J. Mater. Chem. 19 (2009) 5442.
[8] M. Manceau, A. Rivaton, J.L. Gardette, S. Guillerez, N. Lemaître, The mechanism of photo-and thermooxidation of poly(3-hexylthiophene) (P3HT) reconsidered, Polym. Degrad. Stab. 94 (2009) 898–907.
[9] M.O. Reese, A.J. Morfa, M.S. White, N. Kopidakis, S.E. Shaheen, G. Rumbles, D.S. Ginley, Pathways for the degradation of organic photovoltaic P3HT: pcbm based devices, Sol. Energy Mater. Sol. Cells 92 (2008) 746–752.
[10] B. Conings, S. Bertho, K. Vandewal, A. Senes, J. D'Haen, J. Manca, R.A.J. Janssen, Modeling the temperature induced degradation kinetics of the short circuit current inorganic bulk heterojunction solar cells, Appl. Phys. Lett. 96 (2010) 163301.
[11] H.J. Kim, H.H. Lee, J.J. Kim, Real time investigation of the interface between a P3HT: pcbm layer and an Al electrode during thermal annealing, Macromol. Rapid Commun. 30 (2009) 1269–1273.
[12] K. Kawano, R. Pacios, D. Poplavskyy, J. Nelson, D.D.C. Bradley, J.R. Durrant, Degradation of organic solar cells due to air exposure, Sol. Energy Mater. Sol. Cells 90 (2006) 3520–3530.
[13] A. Rivaton, S. Chambon, M. Manceau, J.L. Gardette, N. Lemaitre, S. Guillerez, Light-induced degradation of the active layer of polymer-based solar cells, Poly. Degrad. Stab. 95 (2010) 278–284.
[14] X. Wang, C.X. Zhao, G. Xu, Z.K. Chen, F. Zhu, Degradation mechanisms in organic solar cells: localized moisture encroachment and cathode reaction, Sol. Energy Mater. Sol. Cells 140 (2012) 1–6.
[15] M.O. Reese, S.A. Gevorgyan, M. Jørgensen, E. Bundgaard, S.R. Kurtz, D.S. Ginley, D.C. Olson, M.T. Lloyd, P. Morvillo, Ea Katz, A. Elschner, O. Haillant, T.R. Currier, V. Shrotriya, M. Hermenau, M. Riede, K.R. Kirov, G. Trimmel, T. Rath, O. Inganäs, F. Zhang, M. Andersson, K. Tvingstedt, M. Lira-Cantu, D. Laird, C. McGuiness, S. Gowrisanker, M. Pannone, M. Xiao, J. Hauch, R. Steim, D.M. DeLongchamp, R. Rösch, H. Hoppe, N. Espinosa, A. Urbina, G. Yaman-Uzunoglu, J.B. Bonekamp, A.J.J.M. van Breemen, C. Girotto, E. Voroshazi, F.C. Krebs, Consensus stability testing protocols for organic photovoltaic materials and devices, Sol. Energy Mater. Sol. Cells 95 (2011) 1253–1267.
[16] B. Zimmermann, U. Wurfel, M. Niggemann, Long term stability of efficient inverted P3HT: pcbm solar cells, Sol. Energy Mater. Sol. Cells 93 (2009) 491–496.
[17] S.A. Gevorgyan, M.V. Madsen, B. Roth, M. Corazza, M. Hösel, R.R. Sondergaard, M. Jorgensen, F.C. Krebs, Lifetime of organic photovoltaics: status and predictions, Adv. Energy Mater. 6 (2) (2016) 1501208.
[18] S.A. Gevorgyan, M.V. Madsen, H.F. Dam, M. Jorgensen, C.J. Fell, K.F. Anderson, B.C. Duck, A. Meschellof, E.A. Katz, A. Elschner, R. Roesch, H. Hoppe, M. Hermenau, M. Riede, F.C. Krebs, Interlaboratory outdoor stability studies of flexible roll-to-roll coated organic photovoltaic modules: stability over 10,000 h, Sol. Energy Mater. Sol. Cells 116 (2013) 187–196.
[19] Y.Tamai, H.Ohkita, M.Namatame, K.Marumoto, S.Shimomura, T.Yamanari, S.Ito, Light-Induced Degradation Mechanism in Poly(3-hexylthiophene)/Fullerene Blend Solar Cells, Adv. Energy Mater., 1600171. doi:10. 1002/aenm. 201600171
[20] S.M.H. Rizvi, P. Mantri, B. Mazhari, Traps signature in steady state current-voltage characteristics of organic diode, J. Appl. Phys. 115 (2014) 244502.
[21] A.P. Tyagi (ed.), Solar Radiant Energy Over India, Indian Meteorological Department, Ministry of Earth Sciences, Govt. of India, 2009
[22] N. Chander, A.F. Khan, V.K. Komarala, Improved stability and enhanced efficiency of dye sensitized solar cells by using europium doped yttrium vanadate down-shifting nanophosphor, RSC Adv. 5 (2015) 66057–66066.
[23] M. Glatthaar, M. Riede, N. Keegan, K. Sylvester-Hvid, B. Zimmermann, M. Niggemann, A. Hinsch, A. Gombert, Efficiency limiting factors of organic bulk heterojunction solar cells identified by electrical impedance spectroscopy, Sol. Energy Mater. Sol. Cells 91 (2007) 390–393.
[24] B. Ecker, J. Posdorfer, E. von Hauff, Influence of hole extraction efficiency on the performance and stability of organic solar cells, Sol. Energy Mater. Sol. Cells 116 (2013) 176–181.
[25] I.T. Sachs-Quintana, T. Heumüller, W.R. Mateker, D.E. Orozco, R. Cheacharoen, S. Sweetnam, C.J. Brabec, M.D. McGehee, Electron barrier formation at the organic-back contact interface is the first step in thermal degradation of polymer solar cells, Adv. Funct. Mater. 24 (2014) 3978–3985.
[26] J. Zhao, A. Swinnen, G. Van Assche, J. Manca, D. Vanderzande, B. Van Mele, Phase diagram of p3ht/pcbm blends and its implication for the stability of morphology, J. Phys. Chem. B 113 (2009) 1587–1591.
[27] M. Tessarolo, A. Guerrero, D. Gedefaw, M. Bolognesi, M. Prosa, X. Xu, M. Mansour, E. Wang, M. Seri, M.R. Andersson, M. Muccini, G. Garcia-Belmonte, Predicting thermal stability of organic solar cells through an easy and fast capacitance measurement, Sol. Energy Mater. Sol. Cells 141 (2015) 240–247.
[28] A. Guerrero, H. Heidari, T.S. Ripolles, A. Kovalenko, M. Pfannmöller, S. Bals, L.D. Kauffmann, J. Bisquert, G. Garcia-Belmonte, Shelf life degradation of bulk heterojunction solar cells: intrinsic evolution of charge transfer complex, Adv. Energy Mater. 5 (2014) 1401997.
[29] K. Vandewal, S. Himmelberger, A. Salleo, Structural factors that affect the performance of organic bulk heterojunction solar cells, Macromolecules 46 (2013) 6379–6387.
[30] T.S. Ripolles, A. Guerrero, G. Garcia-Belmonte, Polymer defect states modulate open-circuit voltage in bulk-heterojunction solar cells, Appl. Phys. Lett. 103 (2013) 243306.
[31] M. Nyman, S. Dahlström, O.J. Sandberg, R. Österbacka, Unintentional bulk doping of polymer-fullerene blends from a thin interfacial layer of MoO_3, Adv. Energy Mater. 6 (2016) 1600670.